Water Research 90 (2016) 247–257

Contents lists available at ScienceDirect

Water Research

journal homepage: www.elsevier.com/locate/watres

Transport, retention, and long-term release behavior of ZnO nanoparticle aggregates in saturated quartz sand: Role of solution pH and biofilm coating

Yosep Han [a, 1], Gukhwa Hwang [a, 1], Donghyun Kim [a], Scott A. Bradford [b], Byoungcheun Lee [c], Igchun Eom [c], Pil Je Kim [c], Siyoung Q. Choi [d], Hyunjung Kim [a, *]

[a] Department of Mineral Resources and Energy Engineering, Chonbuk National University, Jeonju, Jeonbuk 561-756, Republic of Korea
[b] USDA, ARS, US Salinity Laboratory, Riverside, CA 92507, USA
[c] Risk Assessment Division, National Institute of Environmental Research, Hwangyeong-ro 42, Seo-gu, Incheon 404-708, Republic of Korea
[d] Department of Chemical and Biomolecular Engineering, KAIST, Daejeon 305-701, Republic of Korea

ARTICLE INFO

Article history:
Received 24 August 2015
Received in revised form
21 November 2015
Accepted 6 December 2015
Available online 17 December 2015

Keywords:
ZnO nanoparticle aggregates
Transport and retention
Long-term release
Biofilm
Solution pH
Saturated quartz sand

ABSTRACT

The transport, retention, and long-term release of zinc oxide nanoparticle aggregates (denoted below as ZnO-NPs) were investigated in saturated, bare and biofilm (*Pseudomonas putida*) coated sand packed columns. Almost complete retention of ZnO-NPs occurred in bare and biofilm coated sand when the influent solution pH was 9 and the ionic strength (IS) was 0.1 or 10 mM NaCl, and the retention profiles were always hyper-exponential. Increasing the solution IS and biofilm coating produced enhanced retention of ZnO-NPs near the column inlet. The enhanced NPs retention at high IS was attributed to more favorable NP-silica and NP-NP interactions; this was consistent with the interaction energy calculations. Meanwhile, the greater NPs retention in the presence of biofilm was attributed to larger roughness heights which alter the mass transfer rate, the interaction energy profile, and lever arms associated with the torque balance; e.g., scanning electron and atomic force microscopy was used to determine roughness heights of 33.4 nm and 97.8 nm for bare sand and biofilm-coated sand, respectively. Interactions between NPs and extracellular polymeric substances may have also contributed to enhanced NP retention in biofilm-coated sand at low IS. The long-term release of retained ZnO-NPs was subsequently investigated by continuously injecting NP-free solution at pH 6, 9, or 10 and keeping the IS constant at 10 mM. The amount and rate of retained ZnO-NP removal was strongly dependent on the solution pH. Specifically, almost complete removal of retained ZnO-NPs was observed after 627 pore volumes when the solution pH was 6, whereas much less Zn was recovered when the eluting solution pH was buffered to pH = 9 and especially 10. This long-term removal was attributed to pH-dependent dissolution of retained ZnO-NPs because: (i) the solubility of ZnO-NPs increases with decreasing pH; and (ii) ZnO-NPs were not detected in the effluent. The presence of biofilm also decreased the initial rate and amount of dissolution and the subsequent transport of Zn^{2+} due to the strong Zn^{2+} re-adsorption to the biofilm. Our study indicates that dissolution will eventually lead to the complete removal of retained ZnO-NPs and the transport of toxic Zn^{2+} ions in groundwater environments with pH ranges of 5–9.

1. Introduction

Metal oxide nanomaterials have been extensively used in a variety of industrial applications. In particular, zinc oxide (ZnO) nanoparticles are widely used as raw materials for products in cosmetic, optical, and chemical industries (Wang and Song, 2006; Mu and Sprando, 2010; Wang et al., 2009). However, studies have shown that ZnO can be toxic to humans, plants, and birds (Adams et al., 2006; Brayner et al., 2006; Lin and Xing, 2007), and that it may be even more toxic when Zn^{2+} ions are released in solution (Xia et al., 2008; Miller et al., 2010; Miao et al., 2010). ZnO nanoparticles quickly dissolve in natural aquatic environments due to their solubility and large specific surface area (Mudunkotuwa et al.,

* Corresponding author.
E-mail address: kshjkim@jbnu.ac.kr (H. Kim).
[1] These authors equally contributed to this manuscript.

http://dx.doi.org/10.1016/j.watres.2015.12.009
0043-1354/

2012). Consequently, ecosystems may be adversely affected by the transport, retention, and subsequent dissolution of ZnO nanoparticles. Information on the transport and fate behavior of ZnO nanoparticles is therefore needed to evaluate the potential environmental and health risks posed by exposure in natural environments (Wiesner et al., 2006).

A number of studies have investigated the influence of various environmental factors on the transport and retention of ZnO nanoparticles. Solution chemistry and organic matter have been identified as crucial factors affecting the transport and retention of ZnO nanoparticles (Jiang et al., 2012a; Petosa et al., 2012; Li and Schuster, 2014; Jiang et al., 2010; Jones and Su, 2014). Biofilms consisting of bacterial clusters embedded in extracellular polymeric substances (EPS) at the soil surface (Sussman et al., 1993), have also been reported to play an important role in the transport and retention of nanoparticles (Tong et al., 2010; Mitzel and Tufenkji, 2014; Lerner et al., 2012; Tripathi et al., 2012). For example, Tong et al. (2010) found that the transport behavior of fullerene (C_{60}) in a sand column decreased in the presence of biofilms. Lerner et al. (2012) investigated the transport behaviors of iron nanoparticles coated with acrylic acid (pnZVI) in porous media, and found that biofilm increase the retention of pnZVI at high ionic strength (25 mM NaCl) as a result of the polymer bridging. Tripathi et al. (2012) reported the effects of biofilms and EPS on the transport and retention of 4 types of nanoparticles in a sand column. The retention of nanoparticles was observed to be improved in the presence of the biofilm regardless of the size of the particles or the type of chemistry for the solution. Unlike the aforementioned works, Mitzel and Tufenkji (2014) measured the mobility of PVP-coated silver (Ag) nanoparticles with the age of the biofilms, and found that sand columns coated with mature biofilms have earlier breakthrough and lower retention of PVP-coated Ag nanoparticles than sand columns coated with younger biofilm or without biofilm, due to an increase of the electrosteric repulsive force between the PVP-coated Ag nanoparticles and the biofilms.

The above studies suggest that biofilms influence the transport of nanoparticles, and this is also true for ZnO nanoparticles. Jiang et al. (2013) found that the retention of bare ZnO nanoparticles in sand increased in the presence of *Escherichia coli* biofilm. However, these packed column tests were conducted at a constant pH of 8, while the pH level for actual surface water or groundwater environments varies over a wide range (e.g., 5.0–9.5) (Kim et al., 2009). Changes in pH can chemically alter ZnO nanoparticles. Indeed, ZnO nanoparticles dissolve in the pH range of groundwater environments, and their solubility increases as the pH decreases (Han et al., 2014). This information implies that retained ZnO nanoparticles may be released to the surrounding environment as dissolved Zn^{2+}, especially at a lower pH. The toxicity of dissolved Zn^{2+} may induce biofilm sloughing, which could potentially trigger additional release and transport of ZnO nanoparticles.

Although the above scenario is very plausible in natural environments, to the best of our knowledge, no study has reported on the long-term release behavior of ZnO nanoparticles under various pH conditions in sand with/without biofilm coatings. Hence, our study was designed to overcome these gaps in knowledge. The transport and retention of ZnO nanoparticle aggregates (denoted below as ZnO-NPs) was studied in packed sand columns with/without a *Pseudomonas putida* (*P. putida*) biofilm coating at a fixed pH of 9, in which almost no ZnO dissolution occurs. The post-release behavior of ZnO-NPs was then evaluated by changing the pH of the background solution. Analyses of the transport and long-term release behavior for ZnO-NPs were conducted using breakthrough curves (BTCs) and retention profiles (RPs). The collected data are needed to accurately assess the long-term risks of ZnO nanoparticles in groundwater environments.

2. Materials and methods

2.1. Porous media and electrolyte solutions

Ultra-pure quartz sand (99.8% SiO_2) with particle sizes ranging from 212 to 855 μm were sieved in U.S. standard stainless steel test sieves (Fisher Scientific), such that the average diameter of the sand particles (d_{50}) was approximately 475 μm. The quartz sand was thoroughly cleaned in order to remove any metal and organic impurities (Redman et al., 2004). The cleaned quartz sand was re-hydrated by boiling the mixture in de-ionized (DI) water (Millipore, Billerica, MA) for at least 1 h prior to wet-packing the column. The zeta potential of crushed porous medium was determined at desired conditions using an Otsuka Zetasizer ELS-Z.

Three pH (6, 9, and 10) and two ionic strength (IS) (0.1 and 10 mM) values were selected to encompass expected ranges in typical groundwater environments (Jewett et al., 1995; Kim et al., 2009). The final pH was adjusted using either 0.1 N HCl or NaOH solution (denoted as an unbuffered condition below). For some conditions, a carbonate buffer (a mixture of 9×10^{-4} M $NaHCO_3$ and 1×10^{-4} M Na_2CO_3) (Delory and King, 1945; Kim et al., 2009) was utilized to increase the pH of the solution (denoted as a buffered condition below). The IS of the solutions was adjusted using NaCl as the background electrolyte. All chemicals were reagent grade (Fisher Scientific).

2.2. ZnO nanoparticles and suspension preparation

ZnO nanoparticles were synthesized using a previously described procedure (Han et al., 2014). This protocol is used to prepare ZnO nanoparticles for commercial cosmetics in South Korea. The Supplementary Information (SI) provides details of the synthesis and characterization procedure for ZnO nanoparticles, and their physical properties under dry conditions (Fig. S1 and Table S1). The protocol used to prepare the ZnO-NP suspension has also been fully described in the SI. The influent suspension that was used in the column experiments described below consisted of 20 mg/L ZnO-NPs at a pH = 9 and IS equal to 0.1 or 10 mM NaCl. The pH 9 solution was selected for initial ZnO-NPs transport tests to minimize dissolution and complexities from Zn^{2+} ions that might have different transport characteristics. The dissolution characteristics of ZnO-NPs are presented in Fig. S2. Influent ZnO-NP suspensions were characterized by measuring their size and zeta potential using a Zetasizer (ELS-Z, Otsuka Eletronics Co., Japan). The measurements were performed right before the column experiments and were repeated 30–40 times at room temperature (25 °C).

2.3. Bacterial culture and biofilm formation in quartz sand column

P. putida (KTCT 1641), a representative soil bacterium (Jost et al., 2010), was provided by the Korea Research Institute of Bioscience and Biotechnology (KRIBB) for biofilm formation. *P. putida* was grown following the protocol provided by the KRIBB. Specifically, they were grown in a nutrient broth medium (Difco) that contained 3.0 g beef extract and 5.0 g peptone per liter, without a pH control. *P. putida* cells were inoculated into 500-ml Erlenmeyer flasks containing 200 ml of sterile medium and cultivated aerobically in an orbital rotary shaker (200 rpm) at 26 °C for 20 h. After growth, the cells were harvested by means of centrifugation (SIF-5000R, Lab companion, South Korea) at 3700 *g* for 15 min and were washed three times with 10 mL of 1 mM NaCl to remove residuals from cell surfaces. Cell pellets were then re-suspended in 5 mL of 1 mM NaCl, and this suspension was used as stock for subsequent characterization and column tests.

In order to develop biofilms in quartz sand column, 9 g quartz sand was put into 50 mL tube with 30 mL *P. putida* suspension (~10^8 cells/mL). The tube was then placed in rotator at 80 rpm and 25 °C for 24 h to allow the bacteria to attach on the sand surface. Columns were packed in small increments (~1.5 cm) with this quartz sand that had been saturated and equilibrated with a suspension of *P. putida*. Mild vibration was applied to the column to minimize any layering or air entrapment. Columns were allowed to settle for 24 h after packing in order to allow the bacteria to tightly attach to the quartz sand. After 24 h, a synthetic nutrient solution (Liu and Li, 2008) was pumped through the columns at a flow rate of 1.5 ml/min for 5 day at room temperature. To ensure the uniform formation and distribution of *P. putida* biofilm inside the column, the direction of the flow injection was switched from upflow to downflow every 12 h (Liu and Li, 2008). The distribution of the biofilm in the column was analyzed using a previously reported procedure (Jiang et al., 2013). Briefly, the column media was evenly dissected into 10 segments, and each segment of the quartz sand was placed into a beaker containing 50 mL NaCl-MOPS (3-(*N*-morpholino)-propanesulfonic acid) solution, composed of 100 mM NaCl and 2.2 mM MOPS in DI water. The pH of the prepared solution was adjusted to 6.9–7.1 using NaOH, and then the bacterial suspension was sonicated in an ultrasonication bath for 10 min, followed by vigorous shaking for 10 s. The cultivable and non-cultivable bacterial number of the *P. putida* biofilm was determined via the pour plate method and using a counting chamber (Bürker–Türk chamber, Marienfeld Laboratory Glassware, Germany) with a phase-contrast microscope (ODEO-2003 triple, IPONACOLOGY). The morphology of biofilm on the quartz sand was examined using a field emission scanning electron microscope (SUPRA 40VP, Carl Zeiss, Germany) and an atomic force microscope (Digital Instruments; Nanoscope IV multimode) in tapping mode, and this result was compared with bare sand. AFM was performed in air mode; the Si cantilever had a spring constant of 2 N/m and a nominal tip apex radius of less than 10 nm. For quantitative analysis, the root-mean-squared (RMS) roughness (Boussu et al., 2005) was determined over an area of 10 μm^2.

2.4. Transport and release experiments

An adjustable column (Omnifit, Boonton, NJ) with an inner diameter of 1.5 cm and a length of 10 cm was used in the transport experiments. The column experiments were conducted at a flow rate of 1.14 mL/min (Darcy velocity = 0.25 cm/min), which is representative of groundwater flow (Chen et al., 2010), using peristaltic pumps (Masterflex L/S, Cole–Parmer Instrument Co., USA). In each column experiment, purified quartz sand was wet packed into the column with an average bed porosity of 0.38 ± 0.01. Once the column was packed, more than 10 pore volume (PV) of DI water was used to flush the column, followed by more than 10 PV of the desired electrolyte solution for equilibration.

Five PV of influent ZnO-NP suspension were injected into the column (bare silica or biofilm-coated sand) in an up-flow mode using peristaltic pumps. The ZnO-NP suspension was sonicated in an ultrasonic water bath every 7 min to prevent aggregation prior to entering the column. Measurement of the size distribution of ZnO-NPs before and after injection confirmed the stability of the suspension (Fig. S3a and b shows data for IS = 0.1 and 10 mM NaCl, respectively). Following the ZnO-NP injection, more than 5 PV of ZnO-NP free electrolyte solution at the same IS and pH were injected into the column, and the column effluent was collected in 15 mL centrifuge glass tubes using a fraction collector. The Zn concentration in the effluent was analyzed using ICP-OES (iCAP 7000DUO, Thermo Scientific).

Following completion of transport experiments, the long-term release and/or dissolution of the retained ZnO-NPs was studied. Specifically, an additional 168 h (627 PV) of ZnO-NP-free solution was injected into the column with the same IS (or the same IS buffer) but at different pH levels (6, 9 and 10). The column effluent was collected at 12 h intervals in a 1 L glass flask. Effluent samples were dissolved in 0.5 N HNO_3, diluted by a factor of 2, and then analyzed by measuring the concentration of Zn via ICP. The concentration of retained ZnO-NPs with depth was determined based on previous works (Jiang et al., 2012a, 2010). Column dissections were performed at selected times during the post release experiments. Briefly, we carefully excavated the quartz sand (or biofilm-coated quartz sand) in 1 cm intervals and then placed it into 50 mL tubes containing 0.5 N HNO_3. The sand and the acid-filled tubes were vigorously shaken, and the concentration of the retained ZnO-NPs was determined using an ICP-OES. The tubes with sand were dried at 90 °C overnight to determine the volume of the liquid and the mass of the sand in each tube. The duplicate transport-release tests were conducted under an aerobic condition (dissolved oxygen concentration ≥ ~97%) for each condition.

The total percentage (M_{total}) of recovered ZnO-NPs was calculated as $M_{e1} + M_{e2} + M_{silica}$ (or $M_{biofilm}$). Here, M_{e1} and M_{e2} denote the percentage of the injected ZnO-NPs that were collected from the effluent during the transport and the release phases, respectively. The M_{silica} and $M_{biofilm}$ represent the percentage of the injected ZnO-NPs that were recovered from the silica and biofilm-coated column dissection.

2.5. DLVO interaction energy calculations

Sphere–sphere and sphere-plate configurations were considered for particle–particle and particle-collector systems, respectively. The retarded van der Waals forces for the sphere–sphere and sphere-plate configuration can be calculated according to Equations (1) and (2) as (Hogg et al., 1966; Haznedaroglu et al., 2009; Gregory, 1981; Han and Kim, 2012):

$$F_{vdw} = -\frac{A_{131} a_{P1} a_{p2} \lambda(\lambda + 22.232h)}{6h^2(a_{P1} + a_{P2})(\lambda + 11.116h)^2} \quad (1)$$

$$F_{vdw} = -\frac{A_{132} a_P \lambda(\lambda + 22.232h)}{6h^2(\lambda + 11.116h)^2} \quad (2)$$

where a_{p1} and a_{p2} refer to the radii of the two interacting nanoparticles, and a_p refers to the radius of the nanoparticle; h is the separation distance between the two nanoparticles (Equation (1)) or between the nanoparticle and the collector surface (Equation (2)); A_{131} is the Hamaker constant for the NP-water-NP system; A_{132} is the Hamaker constant for the NP-water-collector. The combined Hamaker constant for the NP-water-NP system (A_{131}) and the NP-water-collector system (A_{132}) was calculated from the Hamaker constants of the individual materials by using the following equation (Han and Kim, 2012; Jiang et al., 2012b; Israelachvili, 1992):

$$A_{131} = \left(\sqrt{A_{11}} - \sqrt{A_{33}}\right)^2 \quad (3)$$

$$A_{132} = \left(\sqrt{A_{11}} - \sqrt{A_{33}}\right)\left(\sqrt{A_{22}} - \sqrt{A_{33}}\right) \quad (4)$$

where A_{11}, A_{22}, and A_{33} are the Hamaker constants for the ZnO nanoparticles, the collector surface, and water, respectively. The value of $A_{11} = 9.21 \times 10^{-20}$ J (Bergström, 1997) and $A_{33} = 3.70 \times 10^{-20}$ J (Israelachvili, 1992), and these parameter values in Eq. (3) give $A_{131} = 1.23 \times 10^{-20}$ J. The value of $A_{22} = 6.50 \times 10^{-20}$ J for bare silica (Israelachvili, 1992) and

$A_{22} = 6.12 \times 10^{-20}$ J for the biofilm-coated sand (Schafer et al., 1998; Nir, 1977; Rijnaarts et al., 1995). These parameters in Eq. (4) give $A_{132} = 6.96 \times 10^{-21}$ and 6.11×10^{-21} J for the ZnO-water-silica and ZnO-water-biofilm systems, respectively.

The electrostatic double layer forces for the sphere–sphere and sphere-plate configurations can be determined according to the following equations (Hogg et al., 1966; Han and Kim, 2012; Jiang et al., 2012b; Israelachvili, 1992):

$$F_{EDL} = 4\pi\varepsilon_r\varepsilon_0\kappa\frac{a_{p1}a_{p2}}{(a_{p1}+a_{p2})}\zeta_{p1}\zeta_{p2}\left[\frac{\exp(-\kappa h)}{1+\exp(-\kappa h)} - \frac{(\zeta_{p1}-\zeta_{p2})^2}{2\zeta_{p1}\zeta_{p2}}\frac{\exp(-2\kappa h)}{1-\exp(-2\kappa h)}\right] \quad (5)$$

$$F_{EDL} = 4\pi\varepsilon_r\varepsilon_0\kappa a_p\zeta_p\zeta_c\left[\frac{\exp(-\kappa h)}{1+\exp(-\kappa h)} - \frac{(\zeta_p-\zeta_c)^2}{2\zeta_p\zeta_c}\frac{\exp(-2\kappa h)}{1-\exp(-2\kappa h)}\right] \quad (6)$$

$$\kappa = \sqrt{\frac{e^2\sum n_{j0}z_j^2}{\varepsilon_0\varepsilon_r kT}} \quad (7)$$

where ε_0 is the permittivity of vacuum; ε_r is the dielectric constant or relative permittivity of water; ζ_{p1} and ζ_{p2} are the zeta potentials for ZnO-NP 1 and 2, respectively, and ζ_p and ζ_c are the zeta potentials for the ZnO-NP and the collector (bare silica or biofilm surface), respectively. z_j is the ion valence, e is the electron charge, and n_{j0} is the number for the concentration of ions in the bulk solution. Table S3 presents zeta potential and NP size values that were used in DLVO interaction force calculations.

3. Results and discussion

3.1. Transport and retention of ZnO-NPs

Fig. 1 shows the BTCs (a) and the RPs (b) of the ZnO-NPs in the presence and in the absence of biofilms when the IS = 0.1 mM and 10 mM NaCl and the pH = 9. The initial transport behavior of the ZnO-NPs showed no difference in BTC as a result of changes in biofilm and IS, and the small breakthrough amount ranged from 1.3 to 2.1% (Table 1). Significant amounts of ZnO-NP retention were observed in the column inlet area for all experimental conditions. However, the RPs were more hyper-exponential in the presence of biofilm or with a higher level of IS (Fig. 1b).

The interaction energy profiles for NPs–NPs, NPs-silica (quartz sand), and NPs-biofilm surfaces were derived in order to better interpret the RP data shown in Fig. 1b. DLVO interaction energy profiles are presented in Fig. 2. The interaction conditions are found to be favorable when the IS = 10 mM NaCl (Fig. 2b, d, and f). In this case, the injected NPs are expected to deposit into a primary minimum on the surface of deposited NPs, as well as the quartz sand or biofilm. NP-NP interaction provides additional deposition sites and facilitates aggregation at the column inlet that may eventually reduce the size of the pore throats in the sand. Both of these factors can contribute to higher retention of NPs at the column inlet, which supports the observed hyper-exponential RPs (Yang et al., 2012; Cai et al., 2014).

The interaction energy profiles at low IS = 0.1 mM NaCl indicate that NPs-silica and NPs-biofilm interaction were relatively unfavorable with energy barriers of >15 kT (Fig. 2a and e). In this case, diffusion of NPs over this energy barrier is unlikely (Bradford and Torkzaban, 2013; Duffadar and Davis, 2007). One plausible explanation for the significant amounts of NP retention when the IS = 0.1 mM is due to nanoscale roughness which was neglected in the DLVO calculations. All natural surfaces exhibit roughness at some scale (Lohwacharin et al., 2015; Shellenberger and Logan, 2002), and nanoscale surface roughness can significantly reduce the energy barrier to the primary minimum at specific locations (Bradford and Torkzaban, 2013; Hoek and Agarwal, 2006). Indeed, AFM analysis for bare quartz sand shows that the surface of quartz sand exhibits ~33.4 nm scale roughness (Fig. 3c and e). In addition, other factors (e.g, sand surface charge heterogeneity (Chen et al., 2001; Tufenkji and Elimelech, 2005) secondary energy minimum interaction (Tian et al., 2010; Tufenkji and Elimelech, 2005), colloids population heterogeneity (Tufenkji and Elimelech, 2004)) might also influence the retention of NPs under the unfavorable condition (i.e., 0.1 mM). However, the contribution of these mechanisms is unlikely due to the following reasons: i) the quartz sand used in the present study was thoroughly cleaned, so that the presence of sand surface charge heterogeneity is negligible; ii) the depth of secondary energy minimum is very shallow (~0.001 kT), which is not sufficient for NPs retention; iii) we measured the zeta

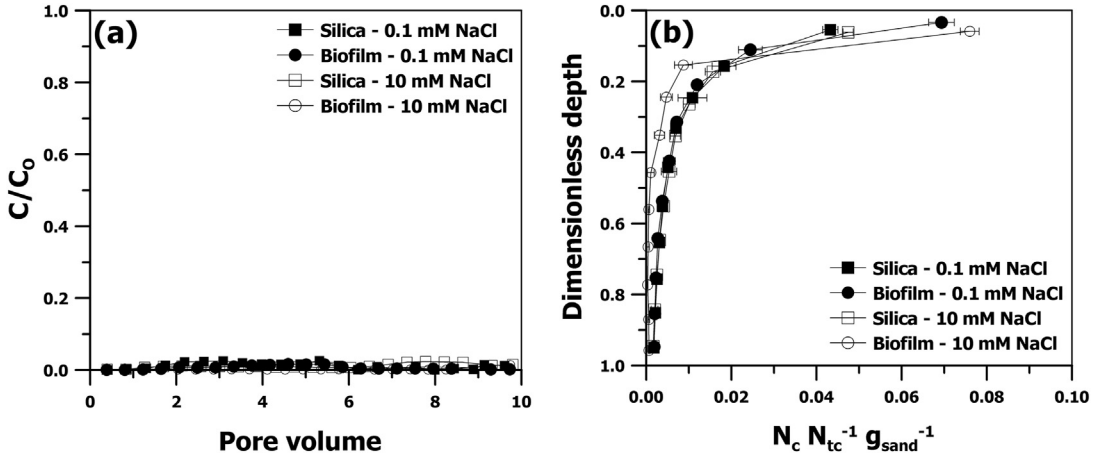

Fig. 1. – Breakthrough curves (a) and retention profiles (b) of ZnO-NPs in the absence and presence of *P. putida* biofilm with different ionic strengths at a pH of 9 in NaCl solutions. C_0 and C represent the influent and effluent ZnO-NPs concentrations, respectively. N_{tc} is the concentration of the ZnO-NPs being injected, and N_c is the concentration of the ZnO-NPs collected by the column dissection at each dimensionless depth.

Table 1
– Mass balance results for ZnO-NPs obtained from column experiments.

Experimental conditions[a]										
	Substrate	Salt type	IS (mM)	pH	$T_{injection}$[a] (h)	M_{e1}[b] (%)	M_{e2}[b] (%)	M_{silica}[c] (%)	$M_{biofilm}$[c] (%)	M_{total}[d] (%)
Initial (0–10 PV)	silica	NaCl	0.1	9	–	2.1(0.2)[e]	–	91.1(2.2)	–	93.2(2.4)
	biofilm	NaCl	0.1	9	–	2.0(0.1)	–	–	91.7(1.8)	93.7(1.9)
	silica	NaCl	10	9	–	2.0(0.3)	–	89.6(3.3)	–	91.6(3.6)
	biofilm	NaCl	10	9	–	1.3(0.8)	–	–	92.5(1.5)	93.8(2.3)
Release (10–627 PV)	silica	NaCl	0.1	6	168	–	93.7(2.9)	2.1(2.5)		95.8(6.6)
	biofilm	NaCl	0.1	6	168	–	95.1(3.6)		2.8(1.6)	97.9(5.2)
	silica	NaCl	10	6	24	–	58.5(2.1)	40.0(4.1)	–	100.5(6.1)
	biofilm	NaCl	10	6	24	–	21.5(2.0)	–	68.1(3.8)	90.9(5.8)
	silica	NaCl	10	6	48	–	83.5(3.8)	12.3(2.2)	–	100.8(6.0)
	biofilm	NaCl	10	6	48	–	66.8(3.2)	–	23.6(1.7)	91.7(4.9)
	silica	NaCl	10	6	168	–	92.0(4.7)	2.5(0.4)	–	96.5(5.1)
	biofilm	NaCl	10	6	168	–	92.2(4.1)	–	2.6(0.3)	96.1(4.4)
	silica	NaCl	10	9	168	–	78.5(3.5)	19.2(2.9)	–	99.7(6.4)
	biofilm	NaCl	10	9	168	–	74.2(4.1)	–	25.1(1.6)	100.6(5.7)
	silica	buffer	10	9	168	–	56.6(3.3)	37.0(2.2)	–	95.6(5.5)
	biofilm	buffer	10	9	168	–	41.7(4.0)	–	49.4(1.3)	92.3(5.3)
	silica	buffer	10	10	168	–	10.3(1.8)	75.1(1.4)	–	87.4(3.2)
	biofilm	buffer	10	10	168	–	9.7(1.1)	–	85.1(2.0)	96.1(3.1)

[a] The injection time of particle-free electrolyte solution after initial transport tests of 10 PV.
[b] M_{e1} and M_{e2} represent the percentage of the ZnO-NPs in the effluent during the initial transport and release phase, respectively.
[c] M_{sand} and $M_{biofilm}$ mean the percentage of the ZnO-NPs recovered by the dissection of the columns packed with bare silica and biofilm-coated sand, respectively, after transport tests.
[d] M_{total} represents the sum of all percentages (i.e., $M_{e1} + M_{e2} + M_{sand}$ for bare silica and $M_{e1} + M_{e2} + M_{biofilm}$ for biofilm-coated sand).
[e] Value in the parenthesis represents standard deviation of replicate.

potential and the size distribution of NPs in column influent and effluent suspensions, and no significant difference was observed between NPs in two suspensions (Table S2). This indicates that NP population heterogeneity in surface charge and size does not play significant role in retention under the unfavorable condition.

The energy barrier for NP-NP interactions on smooth surfaces was relatively low (~8 *kT*) at 0.1 mM IS level, which could be overcome by the thermal diffusion and/or kinetic energy of diffusing NPs (Hahn and O'Melia, 2004). Moreover, results in the literature suggest that nanoscale roughness may completely eliminate this energy barrier in some instances (Bradford and Torkzaban, 2013; Hoek and Agarwal, 2006). As mentioned above, NP-NP interactions also provide a viable explanation for the observed hyper-exponential RPs.

Fig. 1b indicates that biofilm-coated sand produced higher concentrations of retained NPs at the column inlet than uncoated sand at both IS levels. To explain this phenomenon, DLVO interaction energy profiles for NPs-silica and NPs-biofilm at both IS were derived (Fig. 2a and b for NPs-silica and Fig. 2e and f for NPs-biofilm at 0.1 and 10 mM NaCl, respectively). Energy barriers for NPs on biofilm coated sand were comparable to that for NPs on bare quartz at both IS levels (~16 *kT* for 0.1 mM and no energy barrier for 10 mM), indicating that the higher NP retention in the presence of biofilm is unlikely due to differences in energy barrier heights. An alternative explanation was obtained by examining the surface roughness of biofilm-coated sand via SEM and AFM analyses, and the results were compared with bare quartz sand. Both the visualized images from SEM and AFM and the RMS roughness value (Rq = 33.4 nm for bare silica and Rq = 97.8 nm for biofilm-coated sand) indicate an increase in the surface roughness of the quartz sand after biofilm formation (Fig. 3). Previous studies have reported that roughness can enhance the deposition of micro- or nano-sized colloids (Chen et al., 2011; Hoek and Agarwal, 2006; Jiang et al., 2013; Liu and Li, 2008; Shellenberger and Logan, 2002; Tripathi et al., 2012). Roughness can enhance retention by altering the NP mass transfer rate (Saiers and Ryan, 2005), reducing the energy barrier height and the depth of the primary minimum (Bendersky and Davis, 2011; and Bradford and Torkzaban, 2013), and altering the lever arms to reduce to applied hydrodynamic torque and increase the resisting adhesive torque (Bradford et al., 2013; Burdick et al., 2005). In addition, previous studies reported that metal oxide particles can interact with bacterial surface polymers (e.g., EPS, surface macromolecules) via hydrogen bonding (Jiang et al., 2013; Jucker et al., 1998). *P. putida* cells are known to produce EPS (Fang et al., 2011; Wei et al., 2011), and the IR spectra of ZnO-NPs used in our study exhibited surface functional groups (COO-, OH-) (Fig. S1 and Table S1), suggesting that this NPs-EPS interaction is also possible. All of these factors are, therefore, believed to contribute the enhanced retention of NPs at the low IS = 0.1 mM NaCl.

3.2. Long-term release behavior of ZnO-NPs in pH 6 solution

Transport experiments were conducted to study the transport and retention of ZnO-NPs in bare and biofilm coated sand when the influent solution pH = 9 and IS = 0.1 and 10 mM. As discussed above, nearly 100% of the ZnO-NPs were retained in both bare and biofilm coated sand. Release experiments were subsequently conducted on these same columns to examine the fate of the retained ZnO-NPs when exposed to influent solution at pH = 6 and both IS levels for an extended period of time to simulate a sudden drop in pH in natural environments. Fig. 4 shows the effluent concentration of Zn as a function of time after the injection of NPs-free solution at pH = 6 and both IS levels in bare and biofilm coated sand. Zinc was rapidly released right after the injection of pH = 6 solution at both IS levels, and then the effluent concentration slowly decreased over time to the analytic detection limit after ~87 h. Close examination of the release curves indicates that the Zn release rate was initially slower on the biofilm-coated than the bare sand at both IS levels. For instance, when the IS = 10 mM NaCl about 58.5%, 83.5%, and 92% of the retained ZnO-NPs on bare sand was released to the effluent solution after 24, 48, and 93.7 h, respectively. In contrast, about 21.5%, 66.8%, and 92% of the retained ZnO-NPs on biofilm coated sand was released to the effluent solution after 24, 48, and

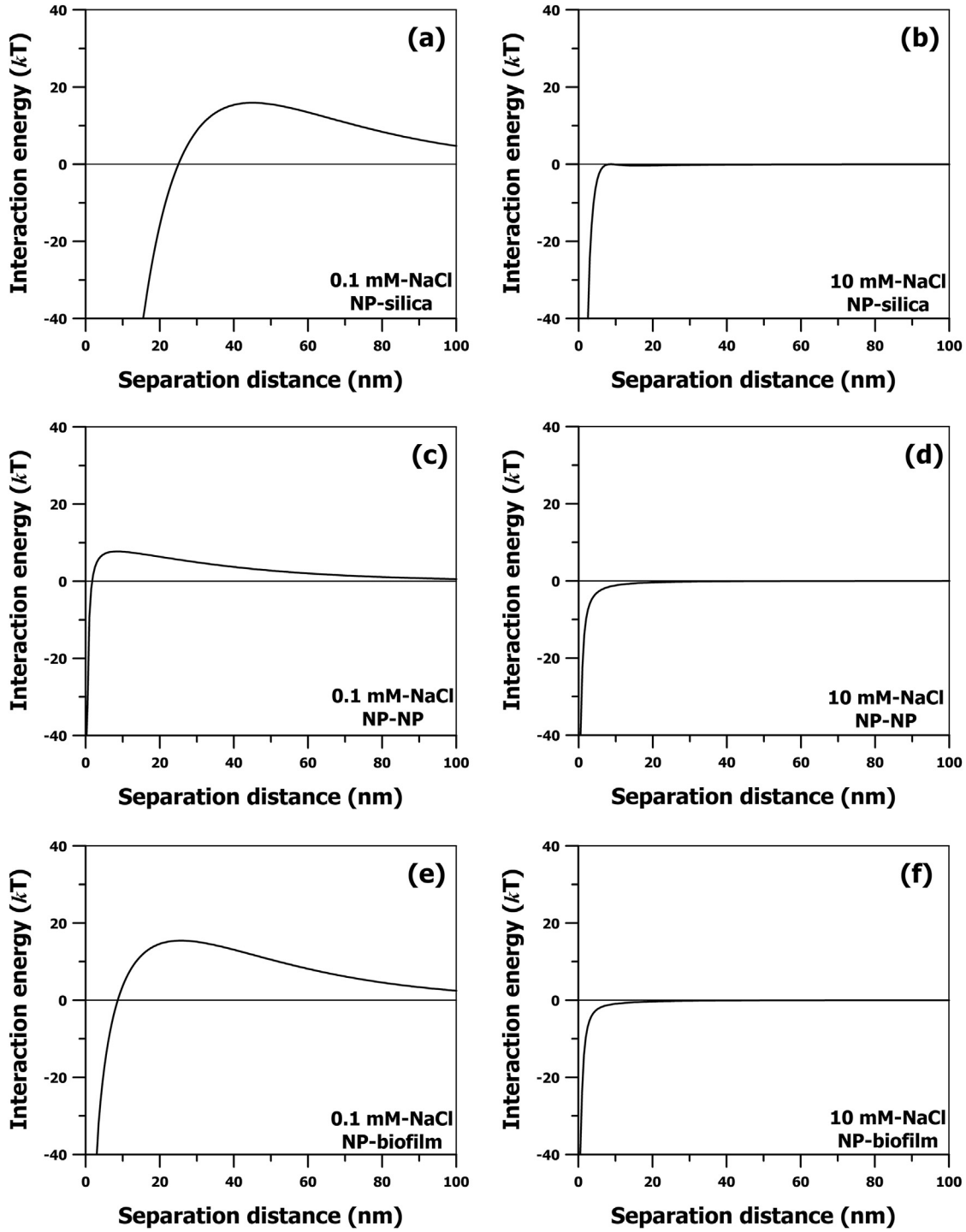

Fig. 2. – DLVO interaction energy profiles for NP-silica (a and b), NP-NP (c and d), and NP-biofilm (e and f) in NaCl solution with 0.1 (a, c, and e) and 10 mM (b, d, and f) IS at pH 9. The measured properties for this calculation are presented in Table S2.

93.7 h, respectively. This observation is further supported in Fig. S4, which presents the initial short-term release behavior of retained ZnO-NPs with and without biofilm. The cause of the slower release of Zn in the presence of biofilm will be discussed later in detail.

Note that the measured concentration of Zn by the ICP does not distinguish between released ZnO-NPs and dissolved Zn^{2+} in the effluent (Fig. 4). Little direct release of ZnO-NPs from the sand to the aqueous phase is expected because conditions are even more favorable of ZnO-NP retention at pH = 6 than pH = 9 (e.g., the isoelectric point (IEP) of ZnO-NPs is pH ~8 (Han et al., 2014) and the magnitude of the zeta potentials of sand decrease with a decrease in pH). Conversely, ZnO-NPs are known to be easily dissolved at a pH of 6 because of a reaction with protons that releases Zn^{2+} (Degen and Kosec, 2000; Yamabi and Imai, 2002; Bian et al., 2011). Less dissolution of ZnO-NPs occurs at pH = 9 because the Zn^{2+} forms hydroxyl complexes on the particle surface (Yamabi and Imai, 2002; Bian et al., 2011; Meulenkamp, 1998). Therefore, a lower pH solution leads to faster ZnO dissolution and higher Zn^{2+}

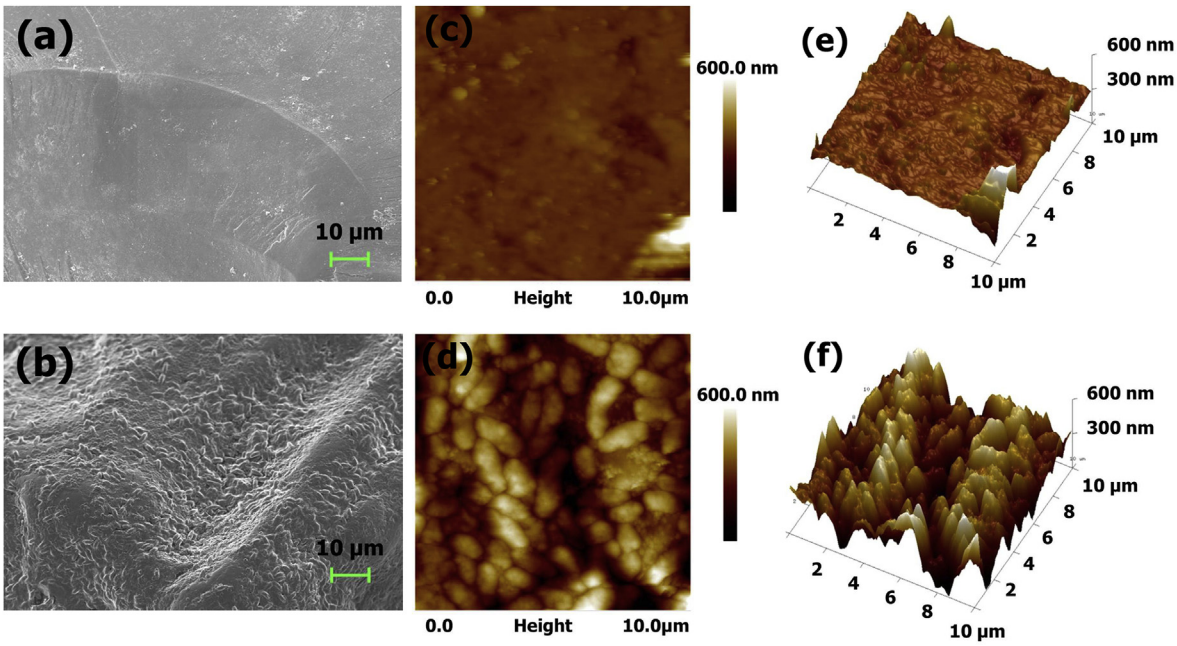

Fig. 3. – FE-SEM (a and b) and AFM (c, d, e, and f) images of bare quartz sand surface (a, c, and e) and *P. putida* biofilm-coated sand surface (b, d, and f).

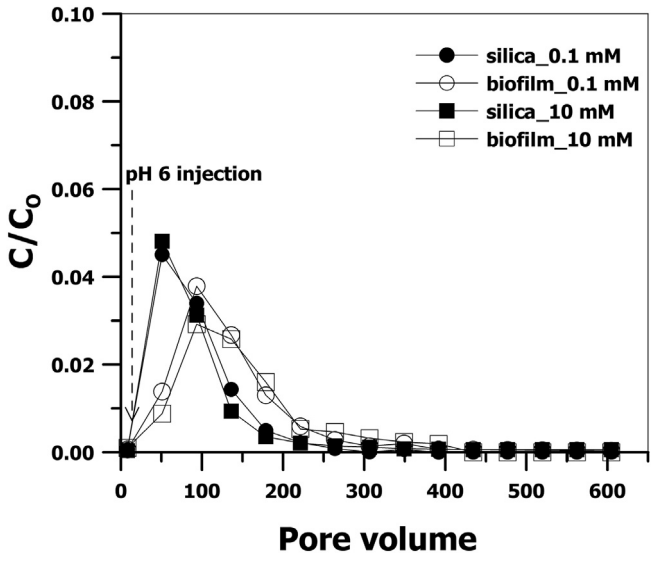

Fig. 4. – Release curves of ZnO-NPs that were initially deposited in 0.1 (circle) and 10 (square) mM NaCl at a pH of 9. These release tests were carried out with particle-free electrolyte solution at pH 6. C_0 and C represent the influent and effluent nanoparticles concentrations, respectively. Note that 0 PV in this graph corresponds to 10 PV in Fig. 1a.

concentrations (Fig. S2). To verify this hypothesis, we compared the Zn concentration of the effluents before and after filtering with a 20 nm pore size syringe filter (Anotop10, Whatman, USA) via ICP analysis, and found almost no difference in the Zn concentration (Table S4). It is worthwhile mentioning that ZnO-NPs did not pass through the 20 nm membrane pores in blank tests (Table S5). Hence, Zn concentration is expected to be higher for unfiltered samples if Zn is present as a particle form, but this is not true for our case. This indicates that Zn concentrations in the effluent of the release experiments were much more dominated by dissolved Zn^{2+} than ZnO-NPs.

The RPs of ZnO-NPs were measured at selected times during the release experiments to gain additional insight on the dissolution process. These measurements were only conducted when the IS = 10 mM NaCl, because similar release behavior was observed at both IS levels (Fig. 4). Fig. 5a and b shows the time lapsed RPs for the bare and the biofilm coated sand when the influent solution pH = 6 and the IS = 10 mM. Dissolution caused the concentration of ZnO-NPs at the top of the column to rapidly decrease with time on both bare and biofilm coated sand. Quantitatively, the amount of retained ZnO-NPs between a dimensionless depth of 0–0.1 decreased to 37.1% and 75.9% on bare and biofilm coated sand, respectively, after 24 h. After 168 h (627 PV) the amount of ZnO-NPs in this region almost vanished (lower than 3%) on both bare and biofilm coated sand (Table 1).

The RPs for ZnO-NPs on bare sand abruptly changed throughout the column after the injection of the pH 6 solution. Conversely, a slight increase in the Zn concentration was observed at dimensionless depths between 0.5 and 1.0 on the biofilm-coated silica after 24 h of injecting solution at pH = 6. This phenomenon continued until 48 h of injection. Furthermore, the Zn^{2+} release rate was also initially slower on the biofilm-coated than the bare sand (Fig. 4 and Fig. S4). These observations suggest that dissolved Zn^{2+} could interact with the biofilm coated sand, and was transported at a slower rate than on bare sand. To verify this hypothesis, we conducted additional column tests using Zn^{2+} in both bare silica and biofilm-coated sand. While almost complete breakthrough was observed in bare silica, negligible NPs transport was detected in biofilm-coated sand (Fig. S5), clearly supporting the conclusion that Zn^{2+} re-adsorbed onto the biofilm presumably due to the binding interaction with reactive molecules (e.g., proteins, polysaccharides, lipids, nucleic acids) that bacterial EPS retain (Guine et al., 2006) and subsequently retards their transport.

3.3. Long-term release behavior of ZnO-NPs in pH 9 and 10 solutions

Additional release experiments were conducted at a

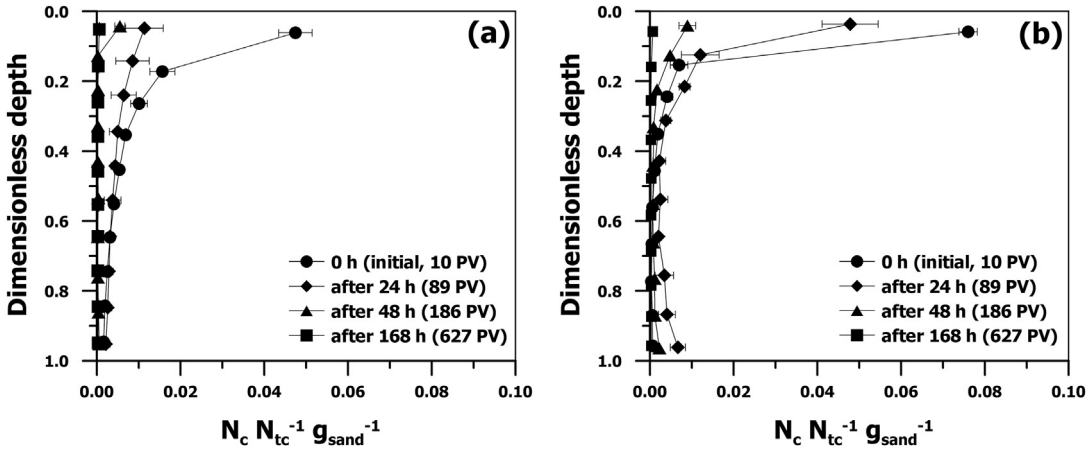

Fig. 5. – Retention profiles of the ZnO-NPs on bare silica (a) and *P. putida* biofilm-coated sand (b) at different times during ZnO-NPs release tests. N_{tc} is the concentration of the ZnO-NPs injected, and N_c is the concentration of the ZnO-NPs collected at each dimensionless depth of a column after release tests. Note that 0 PV in this graph corresponds to 10 PV in Fig. 1a.

representative IS = 10 mM to investigate the effects of pH on the fate of retained ZnO-NPs, and to further confirm that dissolution was the dominant mechanism of release. Fig. 6a shows changes in the effluent concentration of Zn with time in bare and biofilm coated sand when the influent solution pH = 9 and the IS = 10 mM NaCl. Similar to Fig. 4, a greater amount of Zn was initially released from the bare than the biofilm coated sand (Table 1). In contrast to Fig. 4, the peak effluent concentration of Zn was lower and the release rate was slower when the influent solution pH = 9 than pH = 6. This difference in behavior occurs because the solubility of ZnO-NPs decreases as the pH increases (Han et al., 2014). However, the results show that a considerable amount of Zn was still released at pH = 9 (74.2–78.5% after 168 h). This result can be explained by temporal changes in the unbuffered solution pH during transport. Fig. 6c shows that the pH of the effluent decreases from 9 to 7 after 20 h (84 PV) and remains constant until the experiments end at 168 h. This observation suggests that dissolved Zn^{2+} could be released due to temporal pH changes in the column. This hypothesis was tested by repeating the release experiment using influent solution that was buffered to pH = 9 and IS = 10 mM (Fig. 6b). The total amount of Zn that was released after 168 h was much lower in the buffered (41.7–56.6%) than the unbuffered (74.2–78.5%) solutions that were both initially at pH = 9. Furthermore, when an additional release experiment was conducted using influent solution that was buffered at pH = 10 and IS = 10 mM (Fig. 6b), the amount of Zn that was released after a period of 168 h was less than 10.3% (Table 1).

Fig. 7a and b presents the corresponding RPs for ZnO-NPs in bare and biofilm coated sand at the start (initial) and end (168 h) of the release experiments when the influent solution IS = 10 mM and the pH was unbuffered at 9, buffered at 9, and buffered at 10. About 19.2% and 25.1% of the ZnO-NPs remained in the bare and biofilm coated sand after 168 h, respectively, when the influent solution was unbuffered at pH = 9 (Table 1). Conversely, a greater amount of ZnO-NPs remained in the sand after 168 h when the influent solution was buffered to pH = 9 (37–49.4%), and especially when it was buffered to pH = 10 (75.1–85.1%). Furthermore, the shape of the RPs for ZnO-NPs after 168 h was nearly the same as those before the injection when the influent solution pH was buffered at 10.

We measured the bacterial density with distance in the column before and after completion of the release experiments in order to test whether morphological and spatial change of biofilm with column depth occurred over time as a result of lack of nutrients and/or the toxicity of the deposited ZnO-NPs and dissolved Zn^{2+} (Jiang et al., 2013). Fig. S6 shows these results when the influent solution was unbuffered at pH = 9 and the IS = 10 mM. The cultivable and non-cultivable bacterial concentration in the column was almost identical with no significant spatial change before and after the release experiments. Accordingly, the effects of the biofilm sloughing were confirmed to be insignificant.

The above results clearly indicate that the release of ZnO-NPs was not due to the detachment of NPs or sloughing of biofilm, but rather due to dissolution of ZnO-NPs. The amount and rate of dissolution were observed to be a strong function of the solution pH, which increased with decreasing pH.

4. Conclusions

The transport, retention, and long-term release of ZnO-NPs in bare and biofilm coated (*P. putida*) sand were systematically investigated. The retention of ZnO-NPs was found to be enhanced in the presence of biofilms and at higher solution IS. The greater NPs retention in the presence of biofilm could be attributed to larger roughness heights which alter the mass transfer rate, the interaction energy profile, and lever arms associated with the torque balance. This conclusion was supported by scanning electron and atomic force microscopy measurements of the roughness height on bare sand (33.4 nm) and biofilm-coated sand (97.8 nm). Interactions between NPs and EPS may have also contributed to enhanced NP retention in biofilm-coated sand at low IS. Meanwhile, more favorable NP-silica and NP-NP interactions were found to be a crucial factor for the greater NPs retention at higher solution IS regardless of biofilm presence. However, retained ZnO-NPs slowly dissolved and were released as Zn^{2+} back into the aqueous phase over time under environmentally relevant pH conditions (ranging from 5 to 9). The dissolution amount and rate were enhanced at lower pH values that are typical of acid soils because of enhanced solubility of ZnO-NPs, but biofilm coatings slowed the initial release and transport of Zn^{2+} in comparison to bare sand; this trend was mainly attributed to the strong re-adsorption of the released Zn^{2+}-onto the biofilm surface. Results from this study provide valuable insight for evaluating the dissolution behavior and assessing the risks from ZnO-NPs in aquifer environments. Note that, to the best of our knowledge, this is a first study to report the

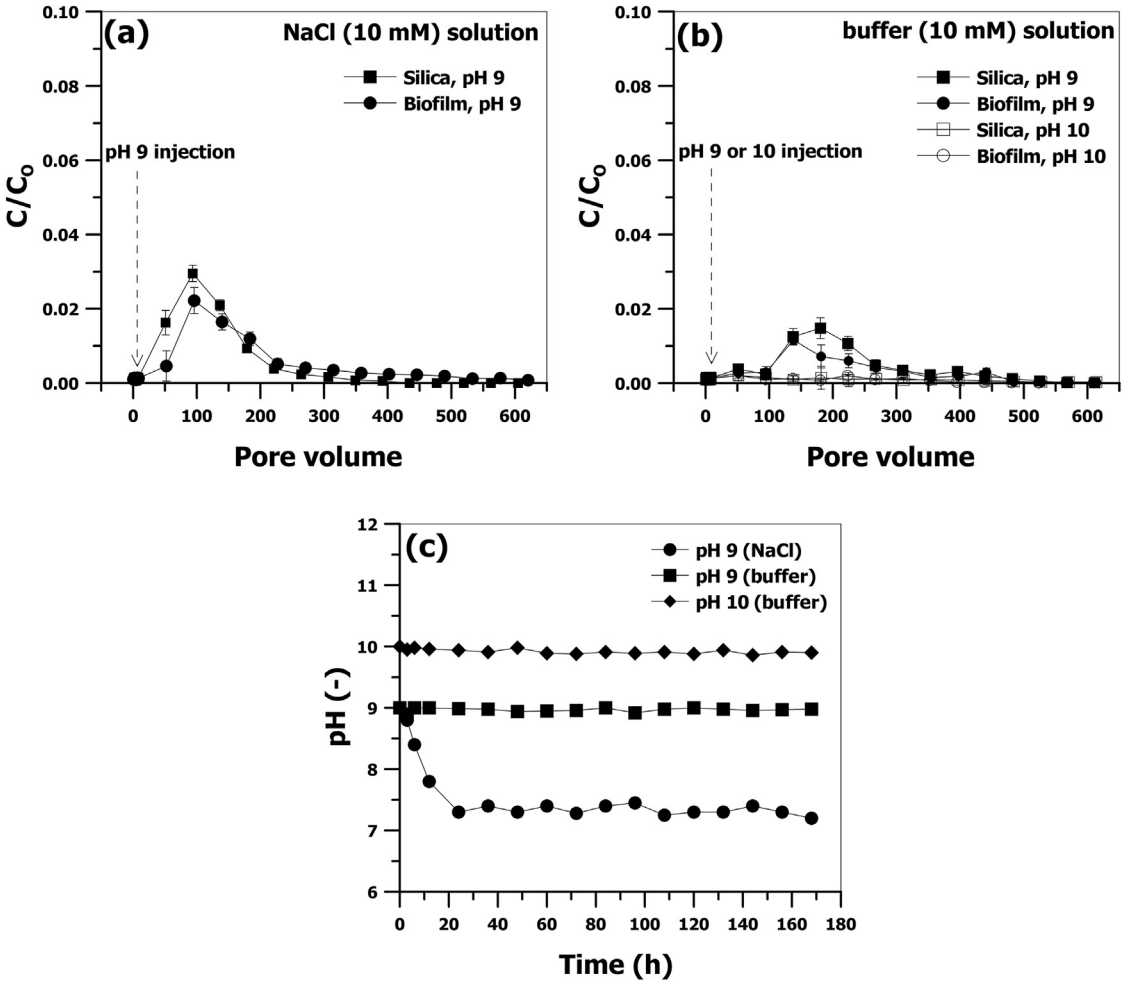

Fig. 6. – Release curves of the ZnO-NPs that were initially deposited in 10 mM NaCl at a pH of 9. These release tests were carried out with a particle-free 10 mM NaCl solution at pH 9 (a) as well as particle-free 10 mM buffer solution at pH 9 and 10 (b). C_0 and C represent the influent and effluent nanoparticle concentrations, respectively. Note that 0 PV in this graph corresponds to 10 PV in Fig. 1a. Change of pH over time for the NaCl solution with initial pH of 9 (circle) and the buffer solutions with initial pH of 9 (square) and 10 (diamond) (c).

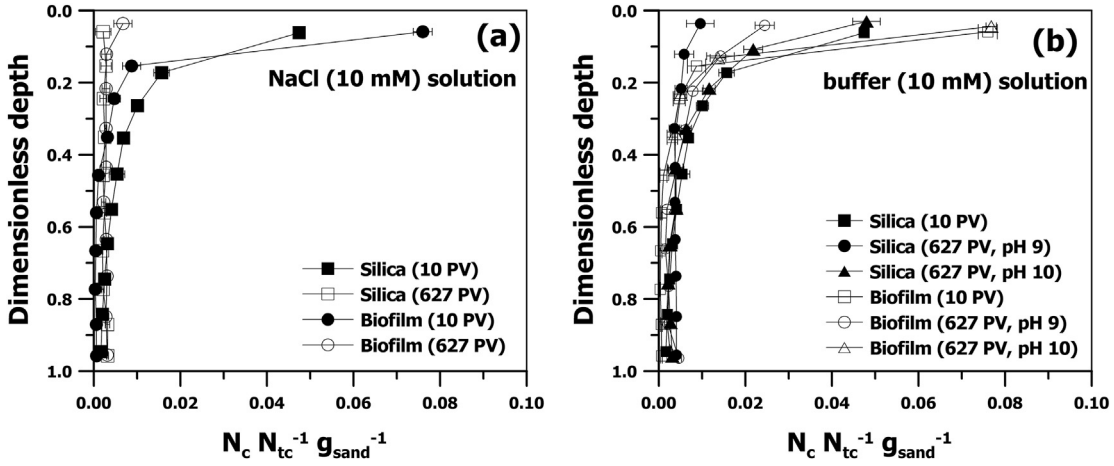

Fig. 7. – Comparison of the retention profiles of the ZnO-NPs on bare silica and *P. putida* biofilm-coated sand after initial (10 PV) and post (10–627 PV) transport tests. N_{tc} is the concentration of the ZnO-NPs injected, and N_c is the concentration of the ZnO-NPs collected at each dimensionless depth of a column after transport/release tests. The retention profiles obtained after initial transport tests are also presented in Fig. 1b.

potential long-term risk of one of the widely used oxide nanoparticles (ZnO nanoparticles) with pH-sensitive solubility due to their transformation over pH change. Further studies on the long-term release and dissolution behavior of other toxic metal oxide nanoparticles, such as CuO, are necessary.

Acknowledgments

This research was supported by the National Institute of Environmental Research, Ministry of Environment of Korea, Basic Science Research Program through the National Research Foundation of Korea funded by the Ministry of Education (NRF-2015020766), and the Ministry of Education (MOE) and National Research Foundation of Korea (NRF) through the Human Resource Training Project for Regional Innovation (2015H1C1A1035930).

Appendix A. Supplementary data

Supplementary data related to this article can be found at http://dx.doi.org/10.1016/j.watres.2015.12.009.

References

Adams, L.K., Lyon, D.Y., Alvarez, P.J.J., 2006. Comparative eco-toxicity of nanoscale TiO_2, SiO_2, and ZnO water suspensions. Water Res. 40 (19), 3527–3532.
Bendersky, M., Davis, J.M., 2011. DLVO interaction of colloidal particles with topographically and chemically heterogeneous surfaces. J. Colloid Interface Sci. 353 (1), 87–97.
Bergström, L., 1997. Hamaker constants of inorganic materials. Adv. Colloid Interface Sci. 70, 125–169.
Bian, S.W., Mudunkotuwa, I.A., Rupasinghe, T., Grassian, V.H., 2011. Aggregation and dissolution of 4 nm ZnO nanoparticles in aqueous environments: influence of pH, ionic strength, size, and adsorption of humic acid. Langmuir 27 (10), 6059–6068.
Boussu, K., Van der Bruggen, B., Volodin, A., Snauwaert, J., Van Haesendonck, C., Vandecasteele, C., 2005. Roughness and hydrophobicity studies of nanofiltration membranes using different modes of AFM. J. Colloid Interface Sci. 286 (2), 632–638.
Bradford, S.A., Torkzaban, S., Shapiro, A., 2013. A theoretical analysis of colloid attachment and straining in chemically heterogeneous porous media. Langmuir 29, 6944–2952.
Bradford, S.A., Torkzaban, S., 2013. Colloid interaction energies for physically and chemically heterogeneous porous Media. Langmuir 29 (11), 3668–3676.
Brayner, R., Ferrari-Iliou, R., Brivois, N., Djediat, S., Benedetti, M.F., Fievet, F., 2006. Toxicological impact studies based on *Escherichia coli* bacteria in ultrafine ZnO nanoparticles colloidal medium. Nano Lett. 6 (4), 866–870.
Burdick, G.M., Berman, N.S., Beaudoin, S.P., 2005. Hydrodynamic particle removal from surfaces. Thin Solid Films 488, 116–123.
Cai, L., Tong, M.P., Wang, X.T., Kim, H., 2014. Influence of Clay particles on the transport and retention of titanium dioxide nanoparticles in quartz sand. Environ. Sci. Technol. 48 (13), 7323–7332.
Chen, G.X., Hong, Y.S., Walker, S.L., 2010. Colloidal and bacterial deposition: role of gravity. Langmuir 26 (1), 314–319.
Chen, G.X., Liu, X.Y., Su, C.M., 2011. Transport and retention of TiO_2 rutile nanoparticles in saturated porous media under low-ionic-strength conditions: measurements and mechanisms. Langmuir 27 (9), 5393–5402.
Chen, J.Y., Ko, C.-H., Bhattacharjee, S., Elimelech, M., 2001. Role of spatial distribution of porous medium surface charge heterogeneity in colloid transport. Colloids Surfaces A Physicochem. Eng. Aspects 191 (1), 3–15.
Degen, A., Kosec, M., 2000. Effect of pH and impurities on the surface charge of zinc oxide in aqueous solution. J. Eur. Ceram. Soc. 20 (6), 667–673.
Delory, G.E., King, E.J., 1945. A sodium carbonate-bicarbonate buffer for Alkaline phosphatases. Biochem. J. 39 (3), 245–245.
Duffadar, R.D., Davis, J.M., 2007. Interaction of micrometer-scale particles with nanotextured surfaces in shear flow. J. Colloid Interface Sci. 308 (1), 20–29.
Fang, L., Wei, X., Cai, P., Huang, Q., Chen, H., Liang, W., Rong, X., 2011. Role of extracellular polymeric substances in Cu (II) adsorption on *Bacillus subtilis* and *Pseudomonas putida*. Bioresour. Technol. 102 (2), 1137–1141.
Gregory, J., 1981. Approximate expressions for retarded van der Waals interaction. J. Colloid Interface Sci. 83 (1), 138–145.
Guine, V., Spadini, L., Sarret, G., Muris, M., Delolme, C., Gaudet, J.P., Martins, J.M.F., 2006. Zinc sorption to three gram-negative bacteria: combined titration, modeling, and EXAFS study. Environ. Sci. Technol. 40 (6), 1806–1813.
Hahn, M.W., O'Melia, C.R., 2004. Deposition and reentrainment of Brownian particles in porous media under unfavorable chemical conditions: some concepts and applications. Environ. Sci. Technol. 38 (1), 210–220.
Han, Y., Kim, D., Hwang, G., Lee, B., Eom, I., Kim, P.J., Tong, M.P., Kim, H., 2014. Aggregation and dissolution of ZnO nanoparticles synthesized by different methods: influence of ionic strength and humic acid. Colloids Surf. A Physicochem. Eng. Asp. 451, 7–15.
Han, Y., Kim, H., 2012. Surface modification of calcium carbonate with cationic polymer and their dispersibility. Mater. Trans. 53 (12), 2195–2199.
Haznedaroglu, B.Z., Kim, H.N., Bradford, S.A., Walker, S.L., 2009. Relative transport behavior of *Escherichia coli* O157:H7 and *Salmonella enterica* serovar pullorum in packed bed column systems: influence of solution chemistry and cell concentration. Environ. Sci. Technol. 43 (6), 1838–1844.
Hoek, E.M.V., Agarwal, G.K., 2006. Extended DLVO interactions between spherical particles and rough surfaces. J. Colloid Interface Sci. 298 (1), 50–58.
Hogg, R., Healy, T.W., Fuersten, Dw, 1966. Mutual coagulation of colloidal dispersions. Trans. Faraday Soc. 62, 1638–1651.
Israelachvili, J.N., 1992. Intermolecular and Surface Forces: with Applications to Colloidal and Biological Systems (Colloid Science).
Jewett, D.G., Hilbert, T.A., Logan, B.E., Arnold, R.G., Bales, R.C., 1995. Bacterial transport in laboratory columns and filters: influence of ionic strength and pH on collision efficiency. Water Res. 29 (7), 1673–1680.
Jiang, X.J., Tong, M.P., Kim, H., 2012a. Influence of natural organic matter on the transport and deposition of zinc oxide nanoparticles in saturated porous media. J. Colloid Interface Sci. 386, 34–43.
Jiang, X.J., Tong, M.P., Li, H.Y., Yang, K., 2010. Deposition kinetics of zinc oxide nanoparticles on natural organic matter coated silica surfaces. J. Colloid Interface Sci. 350 (2), 427–434.
Jiang, X.J., Tong, M.P., Lu, R.Q., Kim, H., 2012b. Transport and deposition of ZnO nanoparticles in saturated porous media. Colloids Surf. A Physicochem. Eng. Asp. 401, 29–37.
Jiang, X.J., Wang, X.T., Tong, M.P., Kim, H., 2013. Initial transport and retention behaviors of ZnO nanoparticles in quartz sand porous media coated with *Escherichia coli* biofilm. Environ. Pollut. 174, 38–49.
Jones, E.H., Su, C.M., 2014. Transport and retention of zinc oxide nanoparticles in porous media: effects of natural organic matter versus natural organic ligands at circumneutral pH. J. Hazard. Mater 275, 79–88.
Jost, D., Winter, J., Gallert, C., 2010. Distribution of aerobic motile and non-motile bacteria within the capillary fringe of silica sand. Water Res. 44 (4), 1279–1287.
Jucker, B.A., Harms, H., Zehnder, A.J., 1998. Polymer interactions between five gram-negative bacteria and glass investigated using LPS micelles and vesicles as model systems. Colloids Surfaces B Biointerfaces 11 (1), 33–45.
Kim, H.N., Bradford, S.A., Walker, S.L., 2009. *Escherichia coli* O157:H7 transport in saturated porous Media: role of solution chemistry and surface macromolecules. Environ. Sci. Technol. 43 (12), 4340–4347.
Lerner, R.N., Lu, Q.Y., Zeng, H.B., Liu, Y., 2012. The effects of biofilm on the transport of stabilized zerovalent iron nanoparticles in saturated porous media. Water Res. 46 (4), 975–985.
Li, L., Schuster, M., 2014. Influence of phosphate and solution pH on the mobility of ZnO nanoparticles in saturated sand. Sci. Total Environ. 472, 971–978.
Lin, D.H., Xing, B.S., 2007. Phytotoxicity of nanoparticles: inhibition of seed germination and root growth. Environ. Pollut. 150 (2), 243–250.
Liu, Y., Li, J., 2008. Role of *Pseudomonas aeruginosa* biofilm in the initial adhesion, growth and detachment of *Escherichia coli* in porous media. Environ. Sci. Technol. 42 (2), 443–449.
Lohwacharin, J., Takizawa, S., Punyapalakul, P., 2015. Carbon black retention in saturated natural soils: effects of flow conditions, soil surface roughness and soil organic matter. Environ. Pollut. 205, 131–138.
Meulenkamp, E.A., 1998. Size dependence of the dissolution of ZnO nanoparticles. J. Phys. Chem. B 102 (40), 7764–7769.
Miao, A.J., Zhang, X.Y., Luo, Z.P., Chen, C.S., Chin, W.C., Santschi, P.H., Quigg, A., 2010. Zinc oxide engineered nanoparticles dissolution and toxicity to Marine phytoplankton. Environ. Tox. Chem. 29 (12), 2814–2822.
Miller, R.J., Lenihan, H.S., Muller, E.B., Tseng, N., Hanna, S.K., Keller, A.A., 2010. Impacts of metal oxide nanoparticles on Marine phytoplankton. Environ. Sci. Technol. 44 (19), 7329–7334.
Mitzel, M.R., Tufenkji, N., 2014. Transport of industrial PVP-stabilized silver nanoparticles in saturated quartz sand coated with *Pseudomonas aeruginosa* PAO1 biofilm of variable age. Environ. Sci. Technol. 48 (5), 2715–2723.
Mu, L., Sprando, R.L., 2010. Application of nanotechnology in cosmetics. Pharm. Res. 27 (8), 1746–1749.
Mudunkotuwa, I.A., Rupasinghe, T., Wu, C.M., Grassian, V.H., 2012. Dissolution of ZnO nanoparticles at circumneutral pH: a study of size effects in the presence and absence of citric acid. Langmuir 28 (1), 396–403.
Nir, S., 1977. Van der Waals interactions between surfaces of biological interest. Prog. Surf. Sci. 8 (1), 1–58.
Petosa, A.R., Brennan, S.J., Rajput, F., Tufenkji, N., 2012. Transport of two metal oxide nanoparticles in saturated granular porous media: role of water chemistry and particle coating. Water Res. 46 (4), 1273–1285.
Redman, J.A., Walker, S.L., Elimelech, M., 2004. Bacterial adhesion and transport in porous media: role of the secondary energy minimum. Environ. Sci. Technol. 38 (6), 1777–1785.
Rijnaarts, H.H., Norde, W., Bouwer, E.J., Lyklema, J., Zehnder, A.J., 1995. Reversibility and mechanism of bacterial adhesion. Colloids Surf. B Biointerfaces 4 (1), 5–22.
Saiers, J.E., Ryan, J.N., 2005. Colloid deposition on non-ideal porous media: the influences of collector shape and roughness on the single-collector efficiency. Geophys. Res. Lett. 32 (21).
Schafer, A., Harms, H., Zehnder, A.J.B., 1998. Bacterial accumulation at the air-water interface. Environ. Sci. Technol. 32 (23), 3704–3712.
Shellenberger, K., Logan, B.E., 2002. Effect of molecular scale roughness of glass beads on colloidal and bacterial deposition. Environ. Sci. Technol. 36 (2), 184–189.
Sussman, M., Denyer, S., Gorman, S., 1993. Microbial Biofilms: Formation and Control. Blackwell Scientific Publication.
Tian, Y., Gao, B., Silvera-Batista, C., Ziegler, K.J., 2010. Transport of engineered nanoparticles in saturated porous media. J. Nanoparticle Res. 12 (7), 2371–2380.
Tong, M.P., Ding, J.L., Shen, Y., Zhu, P.T., 2010. Influence of biofilm on the transport of fullerene nanoparticles in porous media. Water Res. 44 (4), 1094–1103.

Tripathi, S., Champagne, D., Tufenkji, N., 2012. Transport behavior of selected nanoparticles with different surface coatings in granular porous Media coated with *Pseudomonas aeruginosa* biofilm. Environ. Sci. Technol. 46 (13), 6942–6949.

Tufenkji, N., Elimelech, M., 2004. Deviation from the classical colloid filtration theory in the presence of repulsive DLVO interactions. Langmuir 20 (25), 10818–10828.

Tufenkji, N., Elimelech, M., 2005. Breakdown of colloid filtration theory: role of the secondary energy minimum and surface charge heterogeneities. Langmuir 21 (3), 841–852.

Wang, Q., Geng, B.Y., Wang, S.Z., 2009. ZnO/Au hybrid nanoarchitectures: wet-chemical synthesis and structurally enhanced photocatalytic performance. Environ. Sci. Technol. 43 (23), 8968–8973.

Wang, Z.L., Song, J.H., 2006. Piezoelectric nanogenerators based on zinc oxide nanowire arrays. Science 312 (5771), 242–246.

Wei, X., Fang, L.C., Cai, P., Huang, Q.Y., Chen, H., Liang, W., Rong, X.M., 2011. Influence of extracellular polymeric substances (EPS) on Cd adsorption by bacteria. Environ. Pollut. 159 (5), 1369–1374.

Wiesner, M.R., Lowry, G.V., Alvarez, P., Dionysiou, D., Biswas, P., 2006. Assessing the risks of manufactured nanomaterials. Environ. Sci. Technol. 40 (14), 4336–4345.

Xia, T., Kovochich, M., Liong, M., Madler, L., Gilbert, B., Shi, H.B., Yeh, J.I., Zink, J.I., Nel, A.E., 2008. Comparison of the mechanism of toxicity of zinc oxide and cerium oxide nanoparticles based on dissolution and oxidative stress properties. Acs Nano 2 (10), 2121–2134.

Yamabi, S., Imai, H., 2002. Growth conditions for wurtzite zinc oxide films in aqueous solutions. J. Mater. Chem. 12 (12), 3773–3778.

Yang, H.Y., Tong, M.P., Kim, H., 2012. Influence of bentonite particles on representative gram negative and gram positive bacterial deposition in porous Media. Environ. Sci. Technol. 46 (21), 11627–11634.